Constrained optimization of a meander line EMAT generating S0 mode Lamb waves with genetic algorithms

Shen Wang[a] *, Songling Huang[a], Qing Wang[b], Zhe Wang[a] and Wei Zhao[a]

a State Key Lab of Power System, Department of Electrical Engineering, Tsinghua University, Beijing 100084, China

b Department of Engineering, Durham University, DH1 3LE, Durham, UK

Abstract. In this work a Multiphysics model of a meander line electromagnetic acoustic transducer (EMAT) to generate S0 mode Lamb waves in an aluminum plate is built and the structural parameters of the transducer are optimized based on the model. Three approaches to solve the amplitude of the in-plane displacement component at an observation point are explored and the single frequency approach is selected because it is the fastest. In the optimization, the objective function to minimize is the negative amplitude of the S0 mode waves, and the design variables are the width and height of the magnet and liftoff values of the magnet and the coil from the top surface of the plate. The liftoff values form a linear constraint of the optimization problem. A genetic algorithm (GA) program capable of handling the linear constraint efficiency is developed. The internal status of the GA program is tracked carefully to avoid unnecessary evaluations of the objective function. With 30 runs of the program, the optimal set of variables leads to the ratio of the width of the magnet to that of the coil of 115.85%.

Keywords: Ultrasonic transducers, meander line electromagnetic acoustic transducers, Lorentz force, Lamb waves, constrained optimization

1. Introduction

Traditionally in ultrasonic testing, piezoelectric transducers are used to generate ultra- sonic waves in the solid sample under investigation. The piezoelectric transducers rely on liquid coupling to transfer energy into the solid sample, while the coupling is not always convenient 5

* Corresponding author: Shen Wang, State Key Lab of Power System, Department of Electrical Engineering, Tsinghua University, Beijing 100084, China. Email: wangshen@mail.tsinghua.edu.cn

and sometimes uncertainty will be introduced. Several non-contact techniques for generation of ultrasonic waves are promising alternatives, including the laser-generation, air-coupled transducers and electromagnetic acoustic transducers (EMATs). This paper is devoted to the EMATs.

As suggested by the name, EMATs rely on electromagnetic effects to generate ultrasonic waves directly in the tested metal or magnetic sample, without requirement for any liquid coupling [1-3]. In non-magnetic metal testing, the Lorentz force mechanism takes effect. Within the bias magnetic field provided by the permanent magnet, the eddy currents in the metal sample, generated by the coil fed with high frequency excitation current, give rise to the Lorentz forces, serving as the driving forces of the ultrasonic waves. While for magnetic material testing, additional effects like magnetostriction exist, rendering the mechanism even more complex. Only Lorentz force effect is considered for the EMAT described in this paper.

The non-contact nature makes the EMATs suitable for material testing in some special situations, like testing hot or moving samples. Another benefit is that with different configurations of the permanent magnet and the coil, different types of waves could be generated. In spite of these advantages, one difficulty in the use of EMATs is that the energy transduction efficiency is often lower than that of the piezoelectric transducers. So one crucial problem is to design the parameters of the EMATs optimally, so as to maximize their performance.

For optimization of the EMATs, a reliable model is required, while building a model of an EMAT is not an easy task, because the EMAT model is multi-physics in nature, requiring knowledge from both electromagnetic and elastodynamic fields. Ludwig conducted transient analysis of a meander coil EMAT placed on isotropic non-ferromagnetic half-space, assuming uniform static magnetic field [4]. Jafari-Shapoorabadi studied in detail the controlling eddy current equations and argued that the previous work using the total current divided by the cross section area of the conductor as the source current density was equivalently applying the incomplete equation, and this meant ignoring the skin effect and proximity effect [5], while we proved the opposite in [6]. Shi et al. compared three different definitions of the current density with weak formulation [7]. Garcia-Rodriguez et al. implemented both un-coupled and coupled FEM code for EMAT simulations in 2D geometries [8] Dhayalan and Balasubramanniam used FEM package COMSOL to build the electromagnetic model of a meander EMAT, and the simulated Lorentz force was exported to another package Abaqus as the driving force to excite

Lamb waves [9]. The above-mentioned modelling work only involves non-magnetic materials. There is also some initial work on modelling EMATs used to test magnetic material, while we will not discuss further here.

There are already some work on optimizations of EMATs. Mirkhani conducted a parametric study of an EMAT containing a racetrack coil to generate the SV bulk waves propagating perpendicularly into the aluminum sample, by varying the ratio of the width of the magnet to that of the coil, and found that if this ratio was set at 1.2, the amplitude of the ultrasonic beam was improved [10]. One design variable (the width ratio) and one objective function (amplitude of the waves) were used in this optimization, accomplished only through observation of a set of curves corresponding to different design variables instead of using a real optimization algorithm. Kang et al. built a 3D Lamb wave EMAT model in which only the electromagnetic fields were modelled and the orthogonal test method was applied to find an optimal set of input parameters, with Lorentz force components at some selected points as the optimization targets [11]. This process was later extended to a surface wave EMAT model where the surface waves were expressed with existing analytical formulae [12]. The problem of this approach is that the parameters supposed be continuous variables were in fact chosen from respective set of discrete values in an orthogonal test, so they were not fully covered and the mentioned method is not a rigorous mathematical optimization method. Seher et al. optimized a spiral coil EMAT using genetic algorithm optimization procedure in the global optimization toolbox of Matlab [13, 14]. The ratio of the amplitude of the A0 mode to that of the S0 mode is selected as the objective function to be maximized, i.e. preferably generating the A0 mode.

In this paper, we build a 2D model of a meander line EMAT used to generate Lamb waves in an aluminum plate, with the finite element package COMSOL. We choose COMSOL because of its power in multiphysics modelling and great flexibility. This model is based on our previous work [6], while now we focus on the frequency domain model of the EMAT, instead of the time domain model in the previous work. The multiphysics frequency domain model is complete in that the eddy current and the elastic waves are both modeled simultaneously in the frequency domain. This treatment is still rare in the study of EMATs. We discuss different strategies to calculate the amplitude of displacement component at an observation point in the plate, to be used to calculate the objective function in optimizations. We formulate the constrained optimization problem of our meander line EMAT, solved with a genetic algorithm program in

Matlab developed especially for this work. This GA program can handle the linear constraint in our optimization problem efficiently, and we also achieved performance enhancement by decreasing the total number of evaluations of the objective function.

2. The Multiphysics model of a meander line EMAT

In this section we summarise the basic equations in the multiphysics model of a meander line EMAT used to generate Lamb waves in an aluminum plate. The equations come from the electromagnetic and elastodynamic fields. The whole model is divided into the magnetostatic sub-model, the eddy current sub-model and the elastodynamic sub-model, as will be explained in details in section 2.2.

2.1. The controlling equations

The basic equations for the electromagnetic filed simulation in the study of EMATs are Maxwell's equations [15],

$$\nabla x\, E = -\frac{\partial B}{\partial t} \quad (1)$$

$$\nabla x\, H = J_f + \frac{\partial D}{\partial t} \quad (2)$$

$$\nabla \cdot D = \rho f \quad (3)$$

$$\nabla \cdot B = 0 \quad (4)$$

These equations are Faraday's law, Ampere-Maxwell law, Gauss's law for electric fields and Gauss's law for magnetic fields, respectively. **E** is the electric field, **B** is the magnetic flux density, t is the time variable, **H** is the magnetic field strength, $\boldsymbol{J_f}$ is the free current density, **D** is the electric flux density, ρf is the free charge density. ∇x is curl of a vector, and $\nabla \cdot$ is divergence of a vector. Since the frequency in EMAT operation is no higher than several MHz, the term $\frac{\partial D}{\partial t}$ in Maxwell's equations could be neglected.

To solve Maxwell's equations, another set of equations called the constitutive equations are needed,

$$B = \mu H \quad (5)$$

$$D = \in E \quad (6)$$

in which μ is the magnetic permeability, and $\in$ is the dielectric constant. μ and $\in$ are scalars here indicating that the material is linear.

When modeling the magnetic field of the permanent magnet in the magnetostatic simulation, we start from the relation of **B** and **H** in matter,

$$B = \mu_0 (H + M) = \mu_0 (H + x_m H + M_0 = \mu H + \mu_0 M_0 = \mu H + B_r \quad (7)$$

in which $M = x_m H + M_0$ is the magnetization vector, M_0 is the remanent magnetization, and $B_r = \mu_0 M_0$ is the remanent flux density. In region without free currents, (2) is reduced to $\nabla \times H = 0$ and this leads to the definition of magnetic scalar potential V_m as H = -∇V_m . Combing this with (4), we arrive at

$$\nabla \cdot (-\mu \nabla V_m + B_r) = 0 \quad (8)$$

This equation is solved with the magnetostatic sub-model.
With the magnetic vector potential (MVP) A, the equation describing the eddy current phenomenon is,

$$-\frac{1}{\mu}\nabla^2 \boldsymbol{A} + \sigma \frac{\partial \boldsymbol{A}}{\partial t} = J_s \quad (9)$$

in which ∇^2 is the vector Laplacian operator and Js is the source current density, σ is the conductivity. The eddy current density, not written explicitly in (9), is Je = $-\sigma \frac{\partial A}{\partial t}$.This equation holds where there exists a conductor and a source current flows in the conductor.

For 2D planar field simplification where Js is assumed to be along the z axis, we have
Js = Jszez, with Jsz as the z component of vector Js, and ez as the unit vector along the z axis. Similarly we also have A = Azez. If we write Az as A and Jsz as Js, the vector equation (9) is transformed to the z component scalar equation,

$$-\frac{1}{\mu}\nabla^2 A + \sigma \frac{\partial A}{\partial t} = J_s \quad (10)$$

This equation is a diffusion equation describing the eddy current phenomenon. Now the eddy current density is Je = $-\sigma \frac{\partial A}{\partial t}$
The externally applied total current *i* is the surface integral of the total current density, i.e. the sum of the source current density Js and the eddy current density Je,

$$i = \iint_S (J_s + J_e)\, dS \quad (11)$$

In a 2D planar model where the conductor is assumed to be long and straight, Js is uniformly distributed, then together with (10), we have,

$$-\frac{1}{\mu}\nabla^2 A + \sigma \frac{\partial A}{\partial t} = \frac{i + j\omega\sigma \iint_s A\, ds}{S} \quad (12)$$

This is the equation designed a complete in the study of EMAT [16].

For steady state or frequency-domain analysis, the phasor notation is adopted,

$$-\frac{1}{\mu}\nabla^2\dot{A} + \mathrm{j}\omega\sigma\dot{A} = \frac{\dot{i} + \mathrm{j}\omega\sigma \iint_S \dot{A}\, dS}{S} \tag{13}$$

The dots on A and i indicate they are complex phasors. ω is the angular frequency. J is the imaginary unit. This frequency-domain integro-differential equation was proposed by Konrad [17]. Equations (12) and (13) are solved in the eddy current sub-model. It should be noted that (12) and (13) hold for source conductors. In non-source conductors like the metal plate the Js term is dropped, while in non-conducting region the eddy current term is also dropped.

The equations describing the generation and propagation of the ultrasonic waves in an elastic solid are [18].

$$\nabla \cdot T = \rho \frac{\partial^2 u}{\partial t^2} - F \tag{14}$$

$$\mathrm{T} = \mathrm{c} : \mathrm{S} \tag{15}$$

$$\mathrm{S} = \nabla_S \mathrm{u} \tag{16}$$

These equations are equation of motion, Hook's law and strain-displacement relation respectively. T is the stress tensor, $\nabla \cdot T$ is its divergence, ρ is the density, F is the body force density, c is the stiffness tensor, S is the strain tensor, and u is the displacement vector. : is the double dot product of a fourth rank tensor c and a second rank tensor S. ∇_Su is the symmetric part of the gradient of the vector u. It should be noted that the same symbol ρ was also used to represent charge density in Maxwell's equations, and this shouldn't cause misunderstanding in this paper.

For homogenous and isotropic media, we have Navier's equation [19],

$$\mu\nabla^2 u + (\lambda + \mu)\nabla(\nabla \cdot u) = \rho \frac{\partial^2 u}{\partial t^2} - F \tag{17}$$

Here λ and μ are Lamé constants. Like the symbol ρ, the symbol μ was also used to represent the magnetic permeability. For 2D plane strain problems like modeling Lamb waves propagating in a plate, we have components of displacement vector u as u = u (x, y, t), v= v(x, y, t) and w = 0. Navier's equation is solved with the elastodynamic sub-model.

The link between the electromagnetic sub-models and the elastodynamic sub-model is the Lorentz force defined as,

$$\mathbf{F_L = J \times B = J \times (B_0 + B_d)} \tag{18}$$

in which B is the total magnetic flux density composed of the static flux density B_0 of the bias magnet, and the dynamic flux density B_d generated by the excitation coil. Usually for exciting current with moderate magnitude, the B_d term is very small compared with B_0. In transient analysis, we can simulate the dynamic effect directly, while in frequency analysis which we will

use extensively in this work, the dynamic effect is much more difficult to model because we can't multiply two complex phasors, so we will use relatively small excitation currents in this work and neglect the B_d term.

2.2. The meander line EMAT model

As already introduced at the beginning of the section, the meander line EMAT model proposed in this paper consists of three sub-models including a magnetostatic sub-model simulating the bias magnetic field, an eddy current sub-model simulating the distribution of eddy currents and the accompanying skin and proximity effects, and an elastodynamic sub-model simulating the generation and propagation of the Lamb waves. The two electromagnetic sub-models share the same geometry composed of the surrounding air, the permanent magnet, the coil, and the middle section of the aluminum plate. The geometry of the elastodynamic sub-model consists of only the full plate. This design is valid because the eddy currents and the resulted Lorentz forces are concentrated in the local region of the plate just under the coil, so in the electromagnetic sub-models, only the middle section of the plate needs to be considered. The Lorentz forces are transferred to the elastodynamic sub-model as the driving forces of the Lamb waves. By dividing the whole model into two geometries and three sub-models, we obtain some benefits. One advantage is that the structure of the whole model is very clear. Another advantage is that we can apply different meshing rules to the same object (the aluminum plate) in different geometries according to respective underlying physics, thus reducing the total number of elements.

The geometry of the two electromagnetic sub-models is shown in Figure 1. The wires, the plate and the permanent magnet are assumed to be indefinitely long in the z direction so a 2D model is valid. The plate in this geometry is only the middle section of the full plate. This middle section is 300 mm in width and 1 mm in height. The width of the magnet is W_M = 0.1 m and the height is H_M = 0.12 m. The material of the magnet is air, in accordance with example models shipped with COMSOL, with remanent flux density of 1 T along the y direction. The coil is meander line type, composed of seven parallel wires, and the currents in two adjacent wires are in opposite directions. The wires have rectangular cross sections. The widths of the cross sections of the wires are W_W = 2 mm, and the heights are H_W = 1 mm. The horizontal distance between the centers of two adjacent wires is half of the wave length λ, calculated from the phase velocity

C_P of the S0 mode Lamb waves and the frequency f. The frequency for the frequency-domain analysis is 250 kHz, and this frequency is also used as the center frequency of a tone burst excitation signal in the transient analysis. With frequency f =250 kHz and a plate thickness of 1 mm, the phase velocity of the S0 mode as determined from the phase velocity dispersion curves is C_P = 5389.25 m/s, then the wavelength is $\lambda = C_P / f$ =21.557 mm. We developed a Matlab program to produce the dispersion curves. The liftoff from the bottom of the magnet to the top surface of the plate section is l_M = 2 mm. The liftoff from the bottom of the coil to the top surface of the plate section is l_C = 0:5 mm. The conductivity of the aluminum plate is 3.774 x10^7 S/m, and the conductivity of the copper wires of the meander coil is 5.998 x10^7 S/m. The magnetic permeabilities of these two materials are the same as that of the air, i.e. μ_0 =1.2566 x10^{-6}H/m. In the optimizations, W_M, H_M, l_M and l_C will be changed, i.e. used as the design variables, as detailed in section 2.3. A layer of infinite elements is added to the boundary of the air region to increase the modeling accuracy in the magnetostatic analysis and the eddy current analysis. Fillets are added to the sharp corners of the magnet and the wires, so that the singularities are removed, while at the same time the number of elements is also increased.

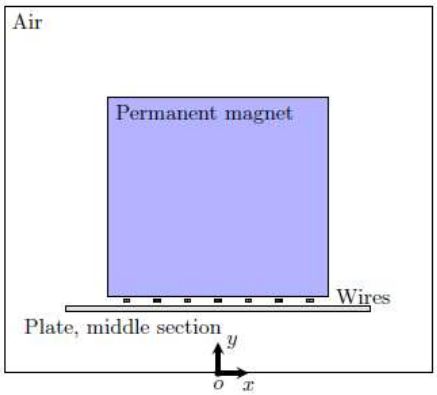

Fig. 1 The geometry of the electromagnetic sub-models (not to scale). This geometry is used for magnetostatic analysis and eddy current analysis

Special care must be taken when meshing the electromagnetic sub-models. For convenience, the plate section is meshed with uniformly distributed rectangular meshes in both the x and y directions, with the mapped method. In the y direction, there are 4 elements in every length of one skin depth (1.6385 x 10^{-4} m for the aluminum material). The copper wires are meshed with 8 boundary layers. The remaining elements are free triangular elements. All the elements have default quadratic shape functions.

The geometry of the elastodynamic sub-model only consists of the full aluminum plate with a total length of 1.2 m. Lamé constants are λ = 5.1 x 10^{10} Pa, and μ = 2.6 x 10^{10} Pa. The density is 2700 kg/m3. In the transient analysis, the ends of the plate are free, and the total time of simulation is limited to avoid end reflection in the recorded waveform of the displacement component. In the frequency domain analysis, PML layers are added to the ends of the plate to allow the wave energy to dissipate, which proves to be a crucial step of modeling. The observation point to record the displacement component is 0.2 m from the center of the transducer and in the middle plane of the plate.

Here we would also like to comment on the dimensions of the EMAT model. Obviously the model proposed in this work is two-dimensional. This model is simpler and mathmatically more mature compared with a 3D model. As a general guideline in finite element method, a 3D model should be avoided until really necessary. For heuristic optimizations with excessive number of evaluations of the numerical model studied in this work, a 3D model is not recommended.

2.3. Parameters to be used as the design variables

In the previous EMAT model, there exist several structural parameters. Among these parameters, some are selected as the design variables of the optimization problem. The design variables are shown in Figure 2. W_M is the width of the permanent magnet, H_M is the height of the magnet, l_M is the liftoff of the magnet from the top surface of the plate, and l_C is the liftoff of the coil/wires from the top surface of the plate. W_M, H_M and l_M are selected because they decide the distribution of the bias magnetic field at the induced eddy currents in the plate. l_C is chosen because it influences the strength of the eddy currents. The two liftoff values are important in EMAT applications because they have big impact to the transduction efficiency of the transducer and hence its performance.

The horizontal distance between the centers of two adjacent wires is fixed at half wavelength of the S0 mode, because we don't want to destroy the matching relation. The widths and heights of the wires are also fixed because we have to limit the number of the design variables and the width of the wire shouldn't be too big because we want accurate matching between the distance of two adjacent wires and the half wavelength.

It should also be noted that the number of wires in the meander coil is fixed at 7 as described in section 2.2. This number is not chosen as a design variable because changing this number means

adding or removing geometrical objects (wires) from a finite element model, and this practice is commonly not advised in optimizations involving complex numerical models.

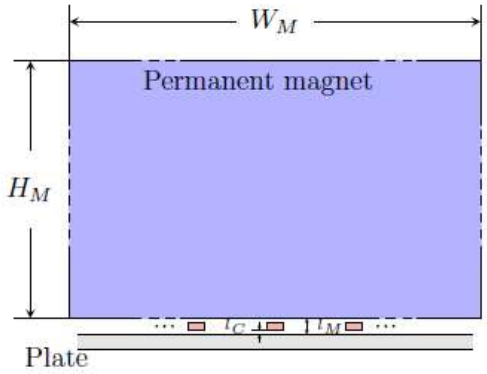

Fig. 2 Design variables of the optimization problem

3. The time domain model vs. the frequency domain model

For optimization, we must obtain the amplitude of the displacement component u at the observation point, since it will be used to calculate the objective function. Deciding how to calculate the amplitude is thus crucial to this work.

The first approach is implemented with the time-domain model, in which the bias magnetic field comes from the magnetostatic simulation while the eddy current distribution, and the generation and propagation of the Lamb waves are from time-dependent simulations. A time-stepping scheme is used for this simulation. For convergence of the time-dependent solver in COMSOL, a very small time step must be used, which means the simulation will be time-consuming. In this work, the number of time steps is set as 8000. The tone-burst excitation signal x(t) is composed of 5 sinusoidal periods and modulated with a Hanning window function. Once the time waveform u(t) at the observation point is simulated, the amplitude/peak of the envelop of this waveform will be solved as,

$$p_u = \mathcal{P}\left(\left|u(t) + \mathrm{i}\mathcal{H}[u(t)]\right|\right) \tag{19}$$

in which i is the imaginary unit, $\mathcal{H}[\cdot]$ is the Hilbert transform, f +j$\mathcal{H}$[f] is the analytic signal corresponding to the time domain signal f, and the absolute value of this analytic signal gives the envelope. $\mathcal{P}$ means solving the peak of the envelope, if there's only one wave packet in the time

waveform, the maximum value of the envelope corresponds to its peak. Because evolutionary algorithms will be applied in this work for optimizations, the number of evaluations of the objective function, i.e. the number of runs of the numerical model, will be big, so the time domain model is too time-consuming to be considered in optimizations, then an alternative faster approach is desired.

The second approach is to transform the input time-continuous excitation signal to its frequency components via Fourier transform (implemented with FFT on a computer), feed them into a frequency domain model, transform the output back into the time-response with inverse Fourier transform (implemented with IFFT), and finally solve the peak of the envelope of the time waveform. The flowchart of this approach is shown in Figure 3. As could be seen in this figure, not all the frequency components are used, and a threshold value is set to select only some of the frequency components with bigger amplitudes. The corresponding subset of the frequencies are input into the frequency model to obtain the system function, then the selected frequency components and the system function are multiplied to obtain the output of the system. Zero paddings in the time domain and the frequency domain are also introduced as optional operations to further increase the calculation accuracy.

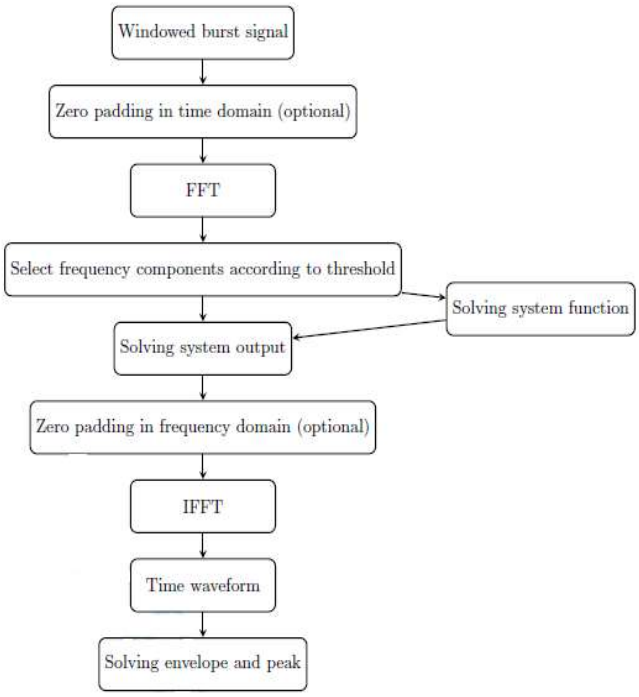

Fig. 3 Flowchart of the FFT/IFFT approach

The time waveform obtained in this way can be expressed as,

$$u(t) = \mathcal{F}^{-1}\{\mathcal{F}[x(t)]H_u(\omega, W_M, H_M, l_M, l_C)\} \quad (20)$$

in which $\mathcal{F}$represents Fourier transform, $\mathcal{F}^{-1}$ is the inverse Fourier transform, x(t) is the input tone burst signal, Hu(ω, W_M, H_M, l_M, l_C) is the system function for the displacement component u. W_M, H_M, l_M and l_C are included to stress that the system function changes with the design variables, while the input signal x(t) is fixed. As the 265 next step, the amplitude/peak is solved just like in Eq.(19). This approach will be less time-consuming than the time-domain simulation, since only tens of (or fewer) frequency components are enough, as selected by the threshold value. For this approach, we build a frequency-domain model of the EMAT, in which the bias magnetic field is again from the magnetostatic simulation, but the eddy current sub-model and the elastodynamic sub-model are completely in the frequency-domain. Then we implement this proposed approach by connecting the frequency-domain model in COMSOL with the Matlab environment. The time waveform from this approach is carefully compared with the waveform from the previous time domain simulation, which serves as a reference. As an example, u waveforms from the time-dependent simulation and the frequency domain model with FFT/IFFT processing are compared in Figure 4. The design variables are selected as W_M = 0.1 m, H_M = 0.12 m, l_M = 0.002 m and l_C = 0.0005 m. The threshold to select the frequency components is 1%, that is, only the frequency components higher than 1% of the peak value of the spectrum are used, and others are discarded. With this threshold, 29 components around the center frequency of 250 kHz are kept.

One important requisite to validate the frequency domain model is that the whole model must be linear. In other words, the frequency model can't handle the part of Lorentz force resulted from the dynamic magnetic field, because two complex phasors cannot be multiplied together to produce another phasor. This is consistent with the discussion about ignoring the B_d term in section 2.1.

Since we are mostly concerned with the amplitude of the u waveform, yet another approach exists, where only one frequency is used in the frequency model, corresponding to a traditional steady state analysis. That is, we only consider the center frequency of the burst signal (250 kHz for the EMAT in this work), and use the absolute value of the complex phasor to approximate the amplitude of the waveform. This process could be formulated as,

$$|\dot{u}| = \left|H_u\left(\omega_c, W_M\, H_M, l_M, l_c\right)\right| \tag{21}$$

in which l_c is the center frequency in radian, $\dot{u}$ is the complex phasor of u.

It's still necessary to prove that the third approach is an acceptable approximation of the second approach. By carefully observing Eq. (21), we can see that $|\dot{u}|$ is the system function evaluated at the center frequency. While in Eq. (20), the spectrum of the tone burst signal $\mathcal{F}\,[x(t)]$ is bell-shaped, i.e. narrow-banded, and concentrated around the center frequency, so the result of $\mathcal{F}^{-1}[\cdot]$ operation is mainly decided by the value of the system function $H_u\left(\omega_c, W_M\, H_M, l_M, l_c\right)$ at the center frequencyω_c, no matter what the system function looks like at other frequencies. Then a higher value of $H_u\left(\omega_c, W_M\, H_M, l_M, l_c\right)$ means higher amplitude of the time waveform, and thus higher peak value of its envelope. So the absolute value of the phasor could be used to approximate the amplitude of the waveform and thus the objective function. Corresponding to Figure 4, the u system function is shown in Figure 5.

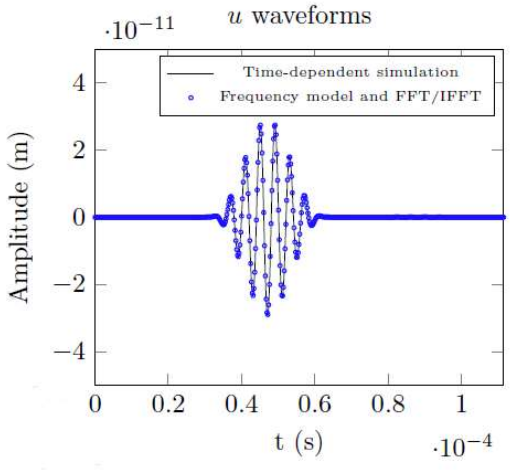

Fig.4 u waveforms from time-dependent simulation and frequency domain model with FFT/IFFT processing

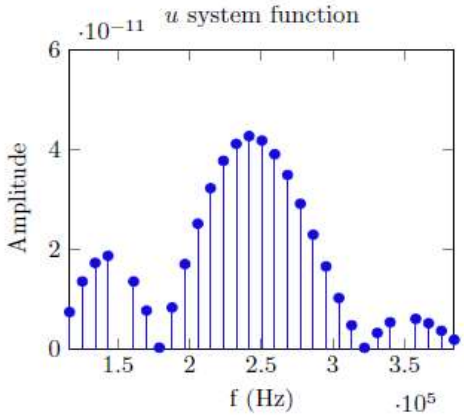

Fig. 5. u system function

The amplitudes of u from the second approach (frequency model with FFT/IFFT) and the third approach (single frequency model) are solved numerically with fixed H_M = 0.12 m, l_M = 0.002 m, l_C = 0.0005 m and different WM values, to further validate the third approach. The results are shown in Figure 6. P_u is the peak value of envelope of u waveform solved with the frequency domain model and FFT/IFFT, while $|\dot{u}|$ is the magnitude of u phasor solved with one single frequency in the frequency domain model. These displacements are recorded at a point away from the transducer and at the middle plane of the plate, as will be explained further. It could be observed that although the amplitudes from these two approaches are not identical, they have same shapes, meaning that they will reach the respective maximum values at similar value of W_M.

The third approach is the fastest, since only one frequency is used. In the later optimizations, we will mainly use this approach.

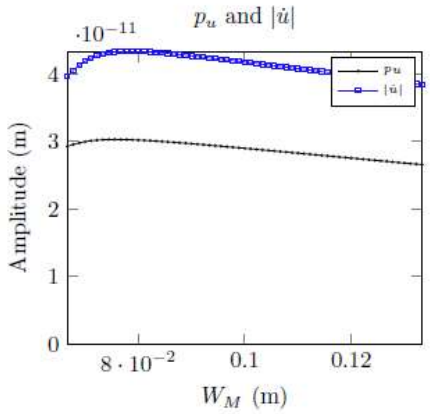

Fig. 6. u amplitudes at different Wm values, from the second and third approaches. H_M = 0.12 m, l_M = 0.002m and l_c = 0.0005 m are fixed

4. Constrained optimization of the meander line EMAT

In this section, we formally present the constrained optimization problem of the meander line EMAT, the features of the developed genetic algorithm program, and the optimization results.

4.1. The constrained optimization problem

Since we are trying to design a transducer to generate the S0 mode Lamb waves, the goal of the optimization is to maximize the amplitude of the S0 mode, or equivalently, minimize the negative of the amplitude of the S0 mode. The optimization problem could be formulated as,

$$\begin{cases} \textbf{minimize } \mathbf{f}(W_M, H_M, l_M, l_C) = -A_{S_0} \\ \textbf{s.t. } l_M - l_C \geq H_W + \delta \end{cases} \tag{22}$$

in which f is the black box FEM model of the meander line EMAT, W_M, H_M, l_M and l_C are the design variables as in section 2.3, AS0 is the amplitude of the S0 mode Lamb waves, H_W = 0.001 m is the height of the wire, δ= 0.0001 m is the lower limit of the air gaps between the bottom of the magnet and the top surface of the wire, and between the bottom of the wire and the top surface of the plate, to avoid that they may intersect with or touch or are too close to each other. The linear contraint in Eq. (22) states that the difference between the liftoff values of the magnet and the coil must accommodate the height of the wire (H_W) and one lower limit of the air gap (δ).

The design variables have upper and lower bounds. If we define the width of the coil as W_C = 0.066671m (3λ+W_W with λ=21.557 mm and W_W=2 mm), then the bounds are $W_M \in [W_C$, 2WC], $H_M \in$ [0:06, 0:16] m, $l_M \in [H_W + 2\,\delta$, 0:015] m, and $l_C \in [\delta$, 0.01] m. The lower bound of W_M is W_C because we want that the magnet could at least cover the coil so that the bias magnetic field is approximately uniform at the coil. The lower bounds of l_M and l_C are easy to select according to geometrical considerations. Other bounds are selected somewhat arbitrarily.

In [14], the authors proposed to solve the displacement components at the middle plane of the plate, then from the displacement wave structures of Lamb waves in a steel plate of 10 mm thickness at 50 kHz, the in-plane component (u) corresponds to the S0 mode only while the out-of-plane component (v) corresponds to the A0 mode only. From our dispersion curves calculation program which also has the ability to solve the wave structures at the selected working point, this is also true for Lamb waves in an aluminum plate with thickness of 1 mm at

250 kHz. So in the FEM model, we record the displacement component u at the observation point in the middle plane of the plate as the S0 mode Lamb waves.

Since the bounds are now defined for the design variables, we can gain some insight of their influences on $|\dot{u}|$ by sweeping one variable while keeping the others constant, based on the previous selection of W_M = 0.1 m, H_M = 012 m, l_M = 0.002 m and l_C = 0:0005 m. Now we sweep them one by one. Figure 7 shows the variation of $|\dot{u}|$ with the width of the magnet W_M, which is the same as the $|\dot{u}|$ curve in Fig. 6, and the only difference is the range of the width value is extended to [30 mm, 129 mm] in Figure 7. Still the peak appears near W_M=80 mm. Figure 8 shows the variation of $|\dot{u}|$ with the height of the magnet ($H_M \in$ [60 mm, 160 mm]). This result shows the bigger is the height of the magnet the larger will be the amplitude of the generated S0 mode waves. Figure 9 is the variation of $|\dot{u}|$ with the liftoff the magnet ($l_M \in [l_C + H_W + \delta$, 14.8 mm]). Figure 10 is the variation of $|\dot{u}|$ with the liftoff of the coil ($l_C \in [\delta$, l_M - H_W -]). These two figures show clearly that smaller liftoff values lead to larger amplitude of the generated S0 mode waves. Although these sweep curves only give an incomplete picture of the influences of the design variables, combined together they show that improvements could be obtained for the optimal design compared with the worst design.

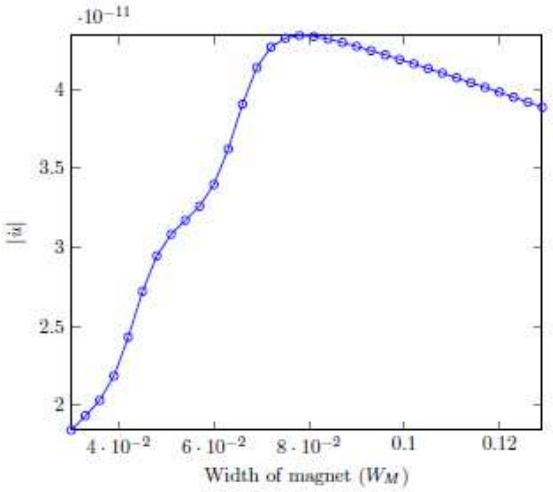

Fig.7. Variation of $|\dot{u}|$ with the width of the magnet

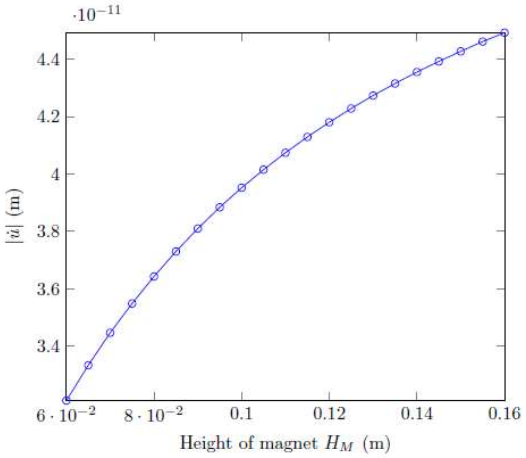

Fig. 8. Variation of $|\dot{u}|$ with the height of the magnet

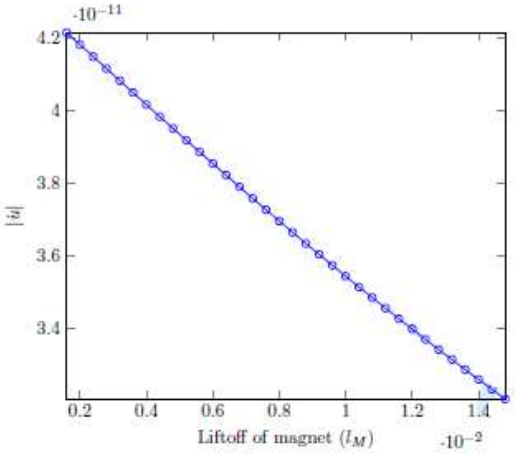

Fig. 9. Variation of $|\dot{u}|$ with the liftoff of the magnet

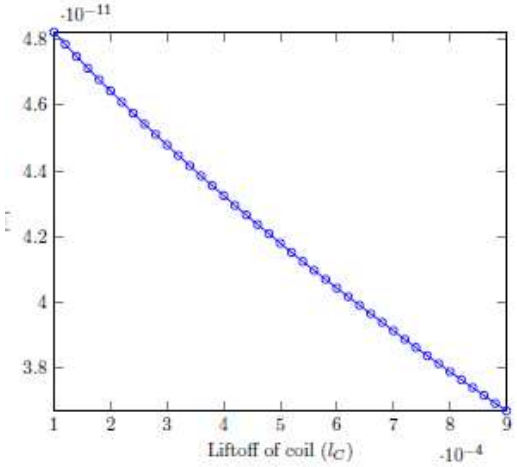

Fig. 10. Variation of $|\dot{u}|$ with the liftoff of the coil

4.2. The genetic algorithm program

For optimization, we choose the genetic algorithm (GA), a kind of global optimization algorithm without requirement to calculate gradients. We developed a genetic algorithm program in Matlab to optimize the parameters of the EMAT, i.e. the design variables. In this program, we implement binary coding and real coding, with or without constraints. The implemented genetic operations are listed as follows,

(1) Uniform mutation
(2) Boundary mutation
(3) Non-uniform mutation
(4) Whole non-uniform mutation
(5) Single arithmetic crossover
(6) Whole arithmetic crossover
(7) Simple crossover
(8) Heuristic crossover

As in Eq. (22), only one linear constraint exists in the optimization problem, and this linearity enables us to handle the constraint efficiently, as proposed in the GENOCOP system developed by Michalewicz [20]. The basic idea is that during the initial phase of the program, all the individuals are generated in the feasible region of the problem. The genetic operations including mutations and crossovers listed above are also carefully customized so that, all the individuals of the new generation also stay in the feasible region.

The program is implemented with object-oriented programming (OOP) technique in Matlab, exploiting the fact that the concepts like individual, population, generation, etc. in GA are naturally modelled with objects in OOP programming paradigm. An advantage of this program is that the total number of evaluations of the objective function is reduced, compared with the code shipped with Matlab itself. This was realized by carefully tracking the internal status of the program and avoiding any unnecessary evaluations. For optimization problems involving complex numerical models, the bottleneck of the optimization procedure is the evaluation of the objective function, or running of the FEM model, so this advantage helps us reduce the total time consumed greatly.

4.3. Optimization results

The single frequency model is used for calculation of the objective function value in the GA program (the third approach). The number of generations is 50, and the number of individuals is

30. 30 runs of the GA program are conducted on a PC running Windows operating system, installed with two Intel Xeon CPUs @ 2.30 GHz, and a RAM of 128 GB. Evolution of the best and mean objective function values versus the number of generation for one run of the program is shown in Figure 11.

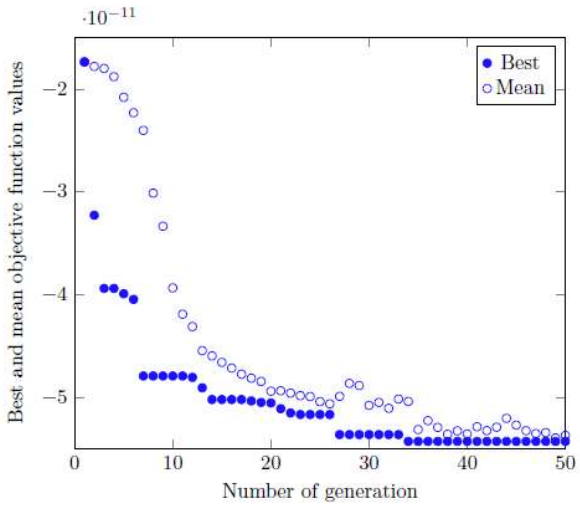

Fig. 11. Best and mean objective function values vs. number of generation for one run of the program

The optimization results of the first 5 runs of the program are summarized in Table 1.

We can observe that the number of evaluations of the objective function changes among the different runs of the GA program. This is normal because we track the internal status of the GA to reduce the number of evaluations, while the internal status of the program is stochastic.

The 30 solved minimized objective function values are sorted in increasing order and drawn in Figure 12. Among the 30 values, the best one (with minimum optimized objective function value) is that the design variables are W_M =77.24 mm, H_M =16 cm, l_M =1.2 mm and l_C =0.1 mm, and the corresponding objective function value is -5.4353 x10^{-11}. The number of evaluations of the objective function (number of runs of the frequency domain model) is 1090, and the total time consumed is 43698 s.[2]

Table 1

Optimization results of the first 5 runs of the program

No.	W_M (m)	H_M (m)	l_M (m)	l_C (m)	Obj function value (m)	Number of evaluations
1	0.078228	0.16	0.0012	0.0001	- 5.4338 x 10^{-11}	1113
2	0.077469	0.15989	0.0012013	0.00010048	- 5.433 x 10^{-11}	1067
3	0.074729	0.15751	0.0012	0.0001	- 5.4139 x 10^{-11}	1127
4	0.076207	0.16	0.0012058	0.0001	- 5.4329 x 10^{-11}	1182
5	0.07732	0.16	0.0012018	0.0001	- 5.4349 x 10^{-11}	1124

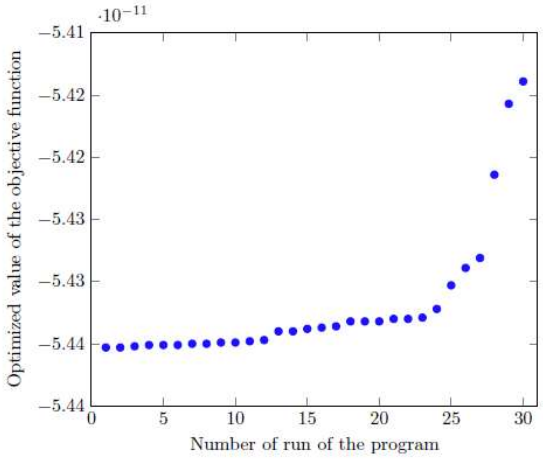

Fig. 12. Optimized value of the objective function of different runs (sorted)

From the results, we can see that H_M reaches the upper bound (0.16 m), this is normal because a bigger value of the height of the magnet corresponds to increased strength of the bias magnetic field. l_M and l_C reach their lower bounds (HW + 2δ = 0.0012 m and δ = 0.0001 m respectively) because smaller value of l_M means increased level of the bias magnetic field and smaller value of l_C means increased level of the dynamic magnetic field and hence the induced eddy currents. We can calculate the value of ratio between the width of the magnet and the width of the coil as W_M=W_C = 115.85%, which is similar to [10], although the structures of the coils are different.

Finally we can compare the amplitude of the displacement component u under optimized variables (W_M=77.24 mm, H_M=16 cm, l_M=1.2 mm and l_C=0.1 mm) with that under the original default variables (W_M=100 mm, H_M=12 cm, l_M=2 mm and l_C=0.5 mm). The time waveforms

from time domain simulations and respective envelopes and peaks of the envelopes (marked with x and +) are shown in Figure 13 (The waveform with bigger amplitude corresponds to the optimized variables). The ratio of the peak with the optimized variables to that with the default variables is 1.3018. We also calculate the ratio of the absolute values of the $\dot{u}$ phasors under the optimized and default variables and find it to be 1.3002. These two ratios are very close. It should be noted that although these ratios show performance improvement of around 30% via optimizations, the values of the ratios depend on the reference/default variables (i.e. a worse set of default variables leads to bigger ratios).

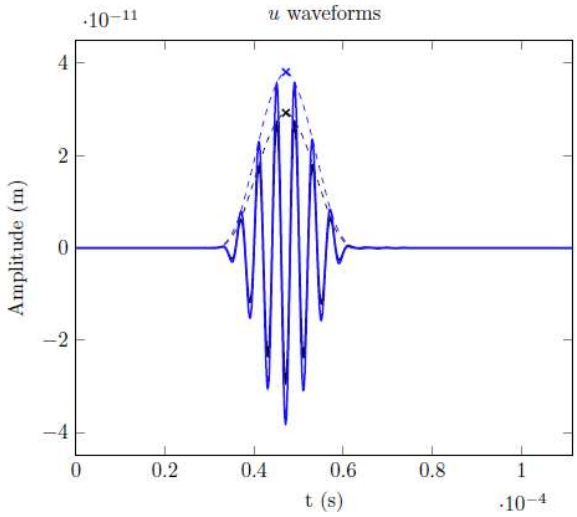

Fig. 13. u waveforms with default and optimized design variables

5. Conclusions

In this work we introduced a 2D model of a EMAT composed of a meander coil and a rectangular magnet used to generate Lamb waves in an aluminum plate. We focus on the complete multiphysics EMAT model in the frequency domain, as the basis of the heuristic optimizations, and this treatment is still rare in the literature on EMATs.

The model was divided into two geometries and three sub-models. The magnetostatic sub-model simulating the bias magnetic field and the eddy current sub-model simulating the distribution of the eddy currents share one geometry while the elastodynamic sub-model simulating the generation and propagation of the Lamb waves has its own geometry. This design has a clear structure, and could ensure that different physics can have different meshing rules, thus reducing the total number of elements.

The quantity we're concerned with is the amplitude of the S0 mode Lamb waves, so this amplitude is used in the optimizations of the EMAT. To obtain the amplitude, three approaches were explored. The first approach is calculating the peak of the envelope of the time waveform from time-domain simulation, which is the most time-consuming. The second less time-consuming approach is also about calculating the peak, but the time waveform is from a frequency domain model, combined with FFT and IFFT processing. The third approach, which is the fastest, is only considering the center frequency in the frequency domain model. This approach was selected for later optimizations implemented with genetic algorithms, so as to greatly reduce the total time of optimization.

The objective function to minimize is the negative amplitude of the S0 mode (i.e. maximising the amplitude of the S0 mode), since we want to strengthen the generation of this mode. The design variables are the width and height of the magnet and liftoff values of the magnet and the coil from the top surface of the plate. The liftoff values form a linear constraint of the optimization problem.

A genetic algorithm program was developed to tackle the problem of optimising the EMAT. This program was implemented with the OOP technique and can handle linear constraint like the one in our optimization problem efficiently. Compared with the code shipped with Matlab, the number of evaluations of the objective functions is reduced. From the optimization results, it was observed that the ratio of the width of the magnet to that of the coil is 115.85%, while the height of the magnet reached its upper limit, and the liftoff values reached respective lower limits.

By comparing the peaks of the envelopes of the u waveforms with the optimized design variables and the original default variables, a performance increase around 30% was observed. Comparing the absolute values of the $\dot{u}$ phasors yielded similar result.

Acknowledgments

The work was finically supported by the National Key R&D Program of China (grant No. 2018YFF0214701) and National Natural Science Foundation of China (grant No. 51777100 and 51677093).

References

[1] RB Thompson. Model for electromagnetic generation and detection of Rayleigh and Lamb waves. *IEEE Transactions on Sonics and Ultrasonics*, **SU20**(4) (1973), 340–346.

[2] RB Thompson. Mechanisms of electromagnetic generation and detection of ultrasonic Lamb waves in iron-nickel alloy polycrystals. *Journal of Applied Physics*, **48**(12) (1977), 4942–4950.

[3] RB Thompson. Model for electromagnetic generation of ultrasonic guided waves in ferromagnetic metal polycrystals, IEEE Transactions on Sonics and Ultrasonics, **25**(1) (1978), 7–15.
[4] R Ludwig and XW Dai. Numerical-simulation of electromagnetic acoustic transducer in the time domain. *Journal of Applied Physics*, **69**(1), (1991), 89–98.

[5] R Jafari-Shapoorabadi, A Konrad, and AN Sinclair. Improved finite element method for EMAT analysis and 340 design. *IEEE Transactions on Magnetics,* **37**(4, 1):2821–2823, JUL 2001. 8th Joint Magnetism and Magnetic Materials International Magnetics Conference (MMM-INTERMAG), San Antonio, Texas, Jan 07-11, 2001.

[6] Shen Wang, Songling Huang, Yu Zhang, and Wei Zhao. Multiphysics modeling of a Lorentz force-based meander coil electromagnetic acoustic transducer via steady-state and transient analyses. *IEEE Sensors Journal*, **16**(17) (2016), 6641–6651.

[7] Wenze Shi, Yunxin Wu, Hai Gong, Zhiran Zhao, Jizhi Fan and Liangchen Tan, Comparison of three formulation for eddy current and skin and proximity problems in a meander coil electromagnetic acoustic transducer, *International Journal of Applied Electromagnetics and Mechanics* **49** (2) (2015), 239-249.

[8] Daniel Garcia-Rodriguez, Ovidiu Mihalache and Masashi Ueda, EMAT simulation based a two-dimensional FEM coupled electro-mechanical formulation, International Journal of Applied Electromagnetics and Mechanics **45**(1-4) (2014), 543-549, 16th International Symposium on Applied Electromagnetics and Mechanics (ISEM), Univ Laval, Pavill Alphonse Desjardins, Quebec City, Canada, Jul 31 – Aug 02, 2013.

[9] R. Dhayalan and Krishnan Balasubramaniam. A hybrid finite element model for simulation of electromagnetic acoustic transducer (EMAT) based plate waves. *NDT & E International*, **43**(6) (2010), 519–526.

[10] K Mirkhani, C Chaggares, C Masterson, M Jastrzebski, T Dusatko, A Sinclair, RJ Shapoorabadi, A Konrad, and M Papini. Optimal design of EMAT transmitters. *NDT & E International*, **37**(3) (2004), 181–193.

[11] Lei Kang, Shujuan Wang, Tao Jiang, and Guofu Zhai. Optimal Design of Lamb Wave Electromagnetic Acoustic Transducers for Improving Their Excitation Performance. *Japanese Journal of Applied Physics*, **50**(7, 2, SI) (2011).

[12] Lei Kang, Steve Dixon, KaicanWang, and Jingmin Dai. Enhancement of signal amplitude of surface wave EMATs based on 3-D simulation analysis and orthogonal test method. *NDT & E International*, **59** (2013), 11–17.

[13] Matthias Seher, Peter Huthwaite, Mike Lowe, Peter Nagy, and Peter Cawley. Numerical design optimization of an EMAT for A0 Lamb wave generation in steel plates. In *40th Annual Review of Progress in Quantitative Nondestructive Evaluation: Incorporating the 10th International Conference on Barkhausen Noise and Micromagnetic Testing*, Vols 33A &33B, D. E. Chimenti, L. J. Bond and D. O. Thompson (eds), AIP Conference Proceedings Vol. 1581. 2014, pp. 340-347.

[14] Matthias Seher, Peter Huthwaite, Michael J. S. Lowe, and Peter B. Nagy. Model-based design of low frequency Lamb wave EMATs for mode selectivity. *Journal of Nondestructive Evaluation*, **34**(3) (2015).

[15] Nathan Ida. *Engineering Electromagnetics*. Springer, 2007.

[16] R Jafari-Shapoorabadi, AN Sinclair, and A Konrad. Finite element determination of the absolute magnitude of

365 an ultrasonic pulse produced by an EMAT. In 2000 IEEE Ultrasonics Symposium Proceedings , Vols 1 and 2, S.C. Schneider, M. Levy and B. R. McAvoy (eds), IEEE Ultrason, Ferroelect, & Frequency Control Soc, 2000, pp. 737-741.

[17] A Konrad. The numerical-solution of steady-state skin effect problems - an integrodifferential approach. *IEEE Transactions on Magnetics*, **17**(1) (1981). 1148–1152.

[18] B. A. Auld, *Acoustic Fields and Waves in Solids*. Krieger Publishing Company, 1990.

[19] Lester W. Schmerr. *Fundamentals of Ultrasonic Nondestructive Evaluation: A Modeling Approach*. Springer, 1998.

[20] Zbigniew Michalewicz, *Genetic Algorithms + Data Structures = Evolution Programs*, Springer, 1998.